Kinetics Analysis of X65 Steel corrosion reactions at the simultaneous presence of CO_2 and H_2S

M. A. Farzaneh *[1], M. Panjepour [2], M. Meratian [3]

Department of Materials Engineering, Isfahan University of Technology

Abstract

In this research, the effect of fluid velocity on corrosion kinetics of X65 steel has been investigated in an aqueous solution containing CO_2 and H_2S according to the steel structures corrosion sensitivity in aqueous environments. The aqueous solution saturated with CO_2 and contained 50 ppm H_2S was used to perform the corrosion tests. The fluid velocity varied between 0 to 1000 rpm, and the tests were carried out at three different temperatures of 298, 318, and 338 K. During the tests, parameters like the iron ion concentration (iron count) (ICP) and instant corrosion rate were monitored. The corrosion products were characterized using XRD and SEM methods and the kinetics and mechanism of the corrosion process were analyzed. The results showed that the first layer, containing mostly mackinawite, does not have the appropriate density, in such a way that the porosities and micro-cracks could be a suitable path for corrosive ions to penetrate the steel surface. Then, as time passed and the thickness of the corrosion product film increased, the number of porosities decreased; this led to the compactness of the product film and resulted in the decrease of diffusion and ion exchange in the interface, and consequently, the corrosion rate decreased.

According to kinetics analysis on the concentration of iron ion variation with time at various temperatures, it was observed that the controlling mechanism of corrosion rate in all the test velocities is of two-dimensional diffusion ($g(\alpha)=(1-\alpha)\ln(1-\alpha)+\alpha$). However, with the increase of fluid velocity, the activation energy of the mentioned diffusion mechanism has increased from 646.47 J/mol to 2743.41 J/mol. In fact, according to the phase analysis and microstructure evaluation of the corrosion products, the reason for this increase could be due to the effect of fluid velocity on the nature and diversity of the corrosion products, especially their continuity and compactness. Therefore, the increase in fluid velocity, at first, resulted in an increase in the corrosion rate, and then, with the formation of a corrosion products layer, its effect has been decreased.

Keywords: Corrosion Mechanism, Carbon Dioxide (CO_2), Hydrogen Sulfide (H_2S), Fluid Velocity, Kinetics Analysis.

1. Introduction

There are several studies related to steel corrosion in aqueous environments containing carbon dioxide (CO_2) [1-4] and hydrogen sulfide (H_2S) as corrosive agents [5, 6]. The mentioned investigations showed that the corrosion products formed on the surface as carbonate and sulfide layers could have a significant effect on the corrosion rate of steel.

Yet, there are several studies about the corrosion mechanisms of steel's in the presence of various gases such as CO_2 or H_2S. For example, Dugstad et al. [2] have investigated the effect of CO_2 on the corrosion behavior of a steel pipes. They found out that the prediction of corrosion behavior of a steel substrate in contact with water containing CO_2 was a complicated issue. Ruhl

**Corresponding author*
Email:farzaneh.me2003@gmail.com
Address:Department of Materials Engineering, Isfahan University of Technology
1. PhD candidate
2. Associate Professor
3. Associate Professor

et al. [7] investigated the corrosion behavior of plain carbon steel in the presence of CO_2. Their results showed that high-alloy steel had a better corrosion resistance compared to plain carbon steel. In similar research, Choi et al. studied the effect of CO_2 concentration on the corrosion behavior of plain carbon steel [8]. Also, Nešić et al. [9] presented a model for predicting the corrosion behavior of plain carbon steel at different temperatures, pHs, and fluid velocities in the presence of CO_2 as a corrosive agent.

On the other hand, various researchers have investigated the effect of H_2S on the corrosion rate of steel. Shoesmith et al. [10] have investigated the effect of H_2S on the formation of iron sulfide. According to their results, the solubility of the H_2S has determined the corrosion rate. Also, Navabzade et al. [11] investigated the effect of the presence of Pyrrhotite [$Fe_{(1-x)}S$] on the corrosion rate of steel. Their results showed that the formation of Pyrrhotite in contact with the steel could result in galvanic corrosion and its rate was dependent on the solution conductivity. In another research, Sun et al. [12] presented a model for predicting the corrosion behavior of plain carbon steel in the presence of H_2S. According to the presented results, the corrosion rate was dependent on the concentration of H_2S, velocity, and the protection degree of the mackinawite layer. There are also some similar studies with similar results [13-14].

Besides the above-mentioned investigations,recently, there is some research on the effect of the individual presence of these gases in particular conditions. For example, Nesic et al. [15] have presented a model to predict the corrosion behavior of plain carbon steels with the presence of CO_2 and H_2S. Moreover, some other models have been presented for predicting the corrosion behavior of plain carbon steel in the presence of these gases. For example, the addition of 100 ppm H_2S has resulted in a decrease in the corrosion rate [16, 17].

Furthermore, the simultaneous presence of these two gases in contact with the steel substrate results in the formation of sulfide and carbonate layers on the surface. According to the obtained results, the nature and thickness of the corrosion product formed on the surface, the fluid movement, and the rate of corrosion product formation, determine the final corrosion rate of the substrate [18, 19]. Despite all the research on this issue and the presented models in current context, there still exists some ambiguities about the effect of fluid movement on corrosion mechanism. For this reason, in the present research, the effect of fluid velocity on corrosion kinetics of X65 plain carbon steel has been studied in a solution containing CO_2 and H_2S as corrosive agents.

2. Materials and Methods

2.1. Materials

In current study, the rectangular x65 steel samples have been used as the substrate with dimensions of 20 mm × 10 mm × 5 mm. The chemical composition of the steel was determined using Optical Emission Spectroscopy (OES) (ARUN 2500) and the results are presented in Table 1.

2.2. Sample Preparations and experimental procedure

The samples were immersed in the solution containing CO_2 and H_2S gases for 28 days. The test solution was daily replaced with a new solution, and the sampling was performed on the replaced solution; this was to simulate the fluid flow in the pipeline and due to continuous displacement of the solution in the pipeline.

The surface roughness of the samples was measured after initial preparation, i.e., grinding and polishing using the Mitutoyo surface profilometer. All the roughness values were around 0.05 μm. According to the effect of fluid velocity on corrosion rate, three rotational speeds of 0, 500, and 1000 revolutions per minute (rpm) (i.e., The Fluid Flow Velocity: 0, 1.2, and 2.4 m/s) were selected for the tests. Since the temperature has a significant effect on the kinetics of the corrosion process, the corrosion evaluations were performed in three different temperatures of 298, 318, and 338 K in the water bath.

Table 1. The chemical composition of X65 steel.

Element	Composition, wt%	Element	Composition, wt%
P	0.009	Al	0.032
Pb	< 0.001	As	0.008
S	0.009	B	0.001
Sb	0.009	C	0.13
Si	0.26	Ca	0.002
Sn	0.07	Co	0.007
Ta	< 0.001	Cr	0.14
Ti	< 0.001	Mn	0.16
V	0.047	Mo	0.16
Zr	< 0.001	Nb	0.017
Fe	Balance	Ni	0.36

To check the repeatability, each test was repeated at least 3 times and the average results are presented in this study. The schematics of the reactor utilized in order to model the effect of fluid flow on corrosion behavior of the X65 steel sample (with the dimension of 1 mm × 2 mm) in the laboratory are shown in Fig. 1. As could be seen in this figure, this reactor includes a stirrer with adjustable speed, pH meter probe, reference electrode,

CO_2 gas purging lance, and a platinum counter. Corrosion measurements were performed using weight loss and LPR techniques for different velocities.

The concentration of CO_2 gas was kept close to saturation concentration by purging 250 ml/min during the tests. The first solution was produced by dissolving different chemical substances as shown in Table 2.

A PerkinElmer AAnalyst 700 atomic absorption apparatus was used to measure the concentration of the iron ion in the solution after 28 days. It is worth noting that in this test system, the concentration of iron ion was considered as the corrosion criteria. For kinetics analysis of the corrosion results, at first, the graphs of iron ion variation with time were plotted at various temperatures and fluid flows, and then, the graphs were converted to reaction fraction graphs.

Besides, the X-Ray Diffraction (XRD), Scanning Electron Microscope (SEM), and Energy Dispersive Spectroscopy (EDS) techniques were used to characterize the corrosion products. In addition, the Potentiostat/ Galvanostat apparatus (EG&G 263A) was used for determining the corrosion rate.

3. Results and discussion

3.1. Corrosion rate analysis

The effect of fluid velocity on the corrosion rate is shown in Fig. 2. According to the results, the general trend is similar for all three fluids, which it means the same corrosion mechanism at these conditions. As seen, the corrosion rate graph has an initial increase followed by a decrease and then gets to a plateau trend with a rate of 5 mpy.

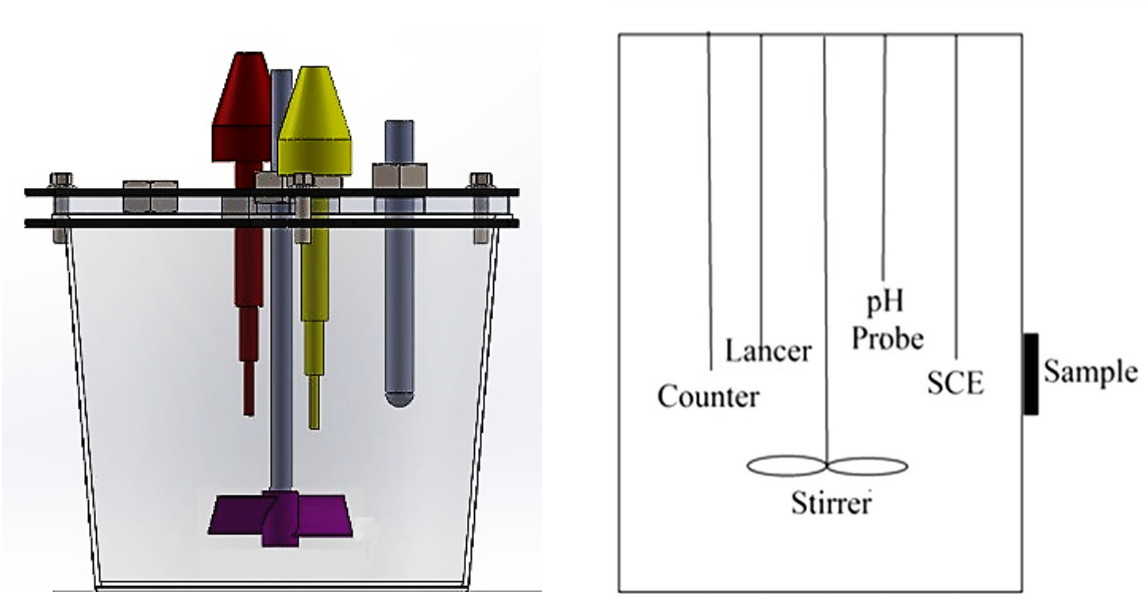

Fig. 1. Schematic and position of electrodes in the corrosion cell.

Table 2. The chemical analysis of the test solution.

Chemical Composition	Quantity (g/L)
$NaHCO_3$	2.75
HCl	3.8
Na_2S	0.5
NaCl	32.5
Water DI	960.45

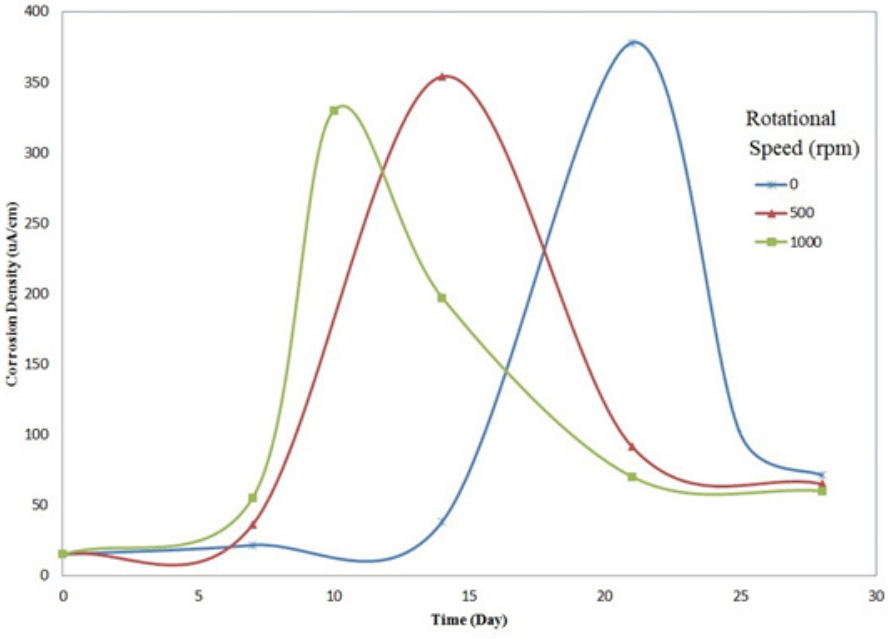

Fig. 2. The variations of corrosion rate versus Time at a different rotational speed.

As the figure shows, an increase in the fluid velocity led to an increase in the slope of the first (the corrosion rate increase) and second (the corrosion rate decrease) steps in such a way that both the mentioned steps would be completed in shorter times. Therefore, the corrosion rate curve becomes plateau in shorter times.

Additionally, the weight loss results are shown in Table 3. According to the results, the corrosion would have a constant rate at higher velocities. In fact, in 1000 rpm, the corrosion rate will be steady after 21 hours, however, for stagnant fluids, it will be going on an increasing rate for extended times even after 21 hours. All the above-mentioned results show the same trend as the current density curves in the figure. It could be said that such behavior is somehow due to the formation of dense and adhesive corrosion products; that are more susceptible to form on higher fluid velocities.

3.2. The effect of surface layers on corrosion

3.2.1. Characterization of corrosion products

The XRD results of the samples are presented in Fig. 3. The results showed that the mackinawite layer is the first layer formed on the surface. Also, as the immersion time increased, the sulfide species converted to other sulfides and caused an increase in sulfide species concentration on the surface. Additionally, the diversity of characterized sulfide species was the same at the surface of all samples in the final stage of the test.

Table 3. The variation of corrosion rate carried out using weight loss method (mm/year).

Time (Day) / Rotational Speed (rpm)	0	7	10	14	21	28
0	0.116	0.116		0.348	4.408	1.044
500		0.406		4.06	1.16	0.986
1000		0.58	3.82	2.436	0.928	0.928

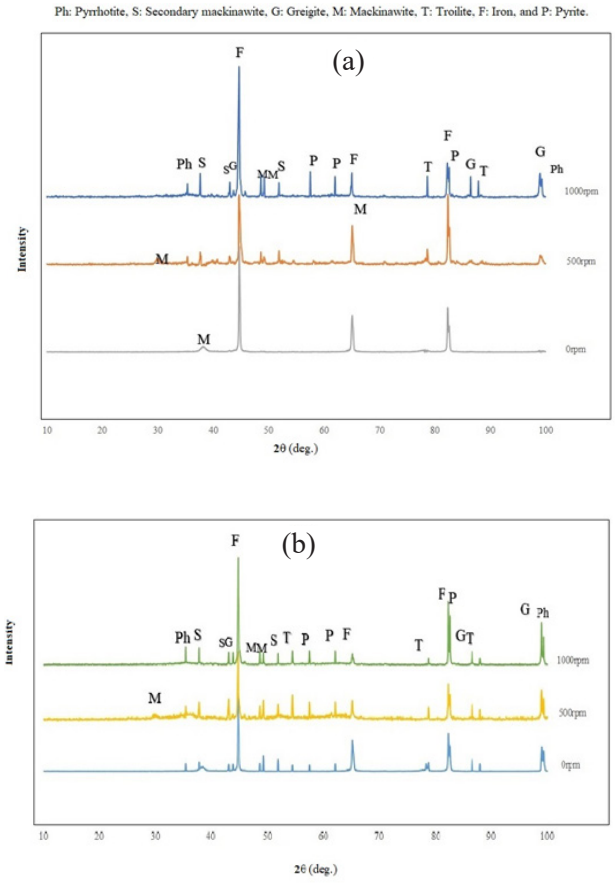

Fig. 3. The XRD Pattern At different times of a) 21 days, b) the 28 days.

As could be seen in the figure, in the stagnant solution, only the mackinawite layer has been identified on the surface after two weeks from the test start. However, other sulfide layers have been identified at the end of the last week. The conditions are quite different for fluids with 500 and 1000 rpm in such a way that all the sulfide layers have formed on the surface on the 21st day. It could be deduced that the formation of compact sulfide layers like pyrite and pyrrhotite can prevent the diffusion of the ions and, as a result, decrease the corrosion rate.

3.2.2. Surface morphology

The SEM micrographs of the sample surface at different Rotational Speed and time is shown in Fig.4. As could be seen in Fig. 4, only one sulfide layer is formed on the surface at the end of the first week. In the images related to the first two weeks, the formed scale has a cubic and acicular structure. It could be seen that the increase in fluid velocity has resulted in diverse sulfide structures and increased the crystal growth rate. Fig. 4 (d to f) shows the SEM micrographs of the surface for various velocities at the end of the 21st day.

Fig. 5 shows the SEM micrographs of the surface after three weeks. In this figure, the sulfide crystals with the dimensions of 1 µm could be observed. Fig. 6 and Fig.7 show the SEM micrographs related to the scale formed on the surface after four weeks. As seen, the formed scale in the stagnant condition is almost uniform, and the acicular sulfide structure and carbonate layers have formed on the surface after four weeks. In this condition, the formed scales had significant growth compared to the previous scales, and the crystals have grown up to 5 µm.

As could be seen in Fig. 7, the length of the formed needles is about 2 µm for the solution with 500 rpm rotational speed after four weeks. Besides, the carbonate crystals with the dimensions of 2 µm can be observed in this figure.

Fig. 7 shows the SEM micrographs of the surface layer (scale) for the solution with 1000 rpm rotational speed and after four weeks. The results of the EDS analysis showed the formation of sulfide and carbonate layers on the surface.

According to the obtained results, which are in conformance with the results of Brown [20], the first layer forming on the surface is mackinawite. The experimental

results also confirm the presence of high amounts of iron sulfide in the surface porosities. This layer does not prevent the diffusion of aggressive ions to the substrate or the metallic ions into the bulk solution due to its acicular structure. As a result, it does not have protective properties against corrosion.

In this condition, i.e., the presence of the mackinawite layer on the surface, the micro-cracks act as the fast diffusion paths for aggressive ions and result in the increased corrosion rate of the substrate, following Schutze's results [21]. Besides, the crack growth due to the growth of the mackinawite layer (Fig.7) leads to the increased transfer rate of sulfide species to the internal interface via these micro cracks. As mentioned before, the nucleation and growth of the cracks on the surface are due to the high Pilling-Bedworth (P-B) ratio (R_{PB}). According to the Dugstad et al. results [2], with the passage of time, these cracks could lead to the detachment of the layer from the substrate unless the sulfide layers convert to other sulfide species.

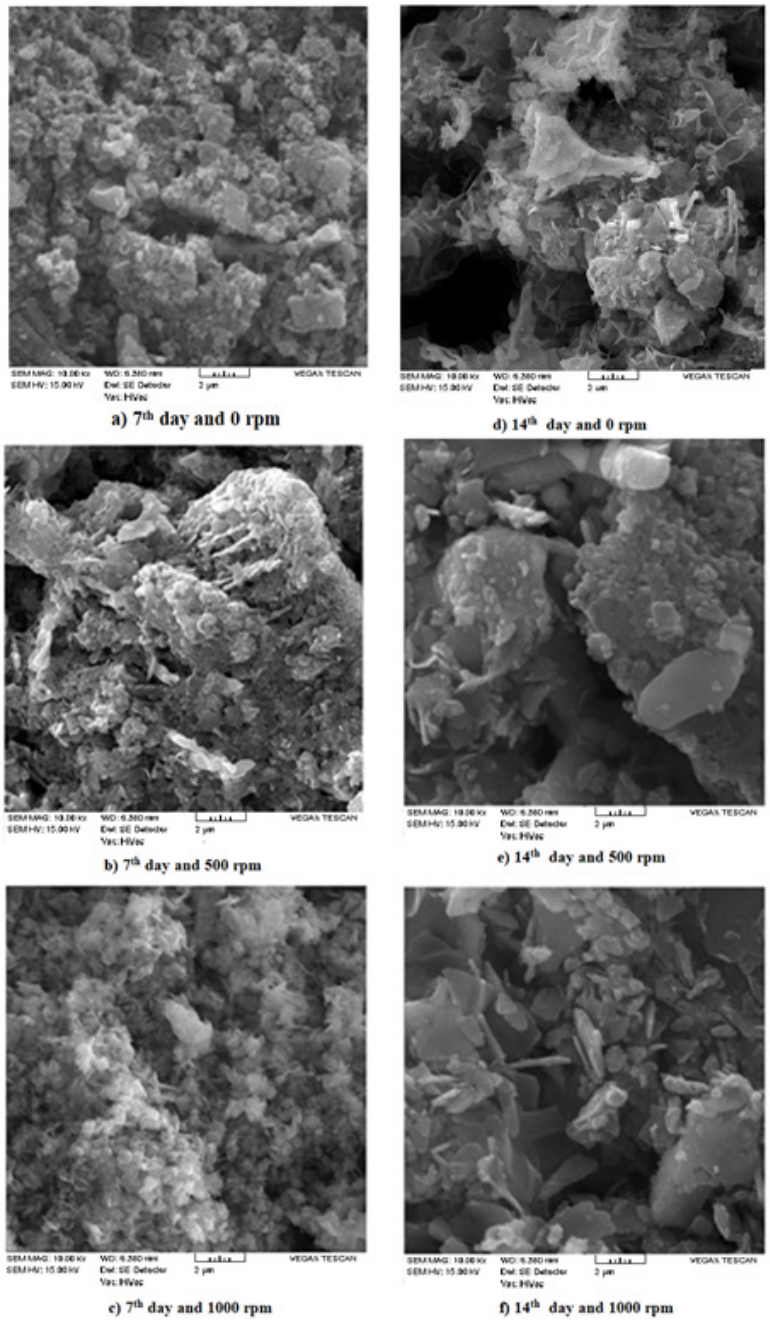

Fig. 4: SEM micrographs of the sample surface at different Rotational Speeds and times.

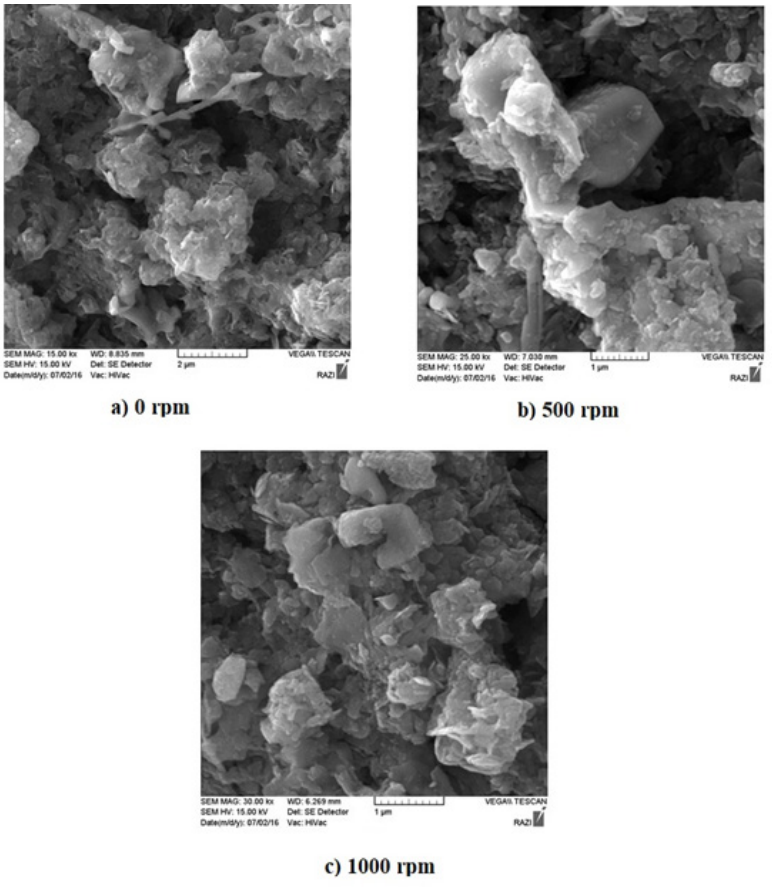

Fig. 5. SEM micrographs of the sample surface on the 21st day and for different rotational Speeds.

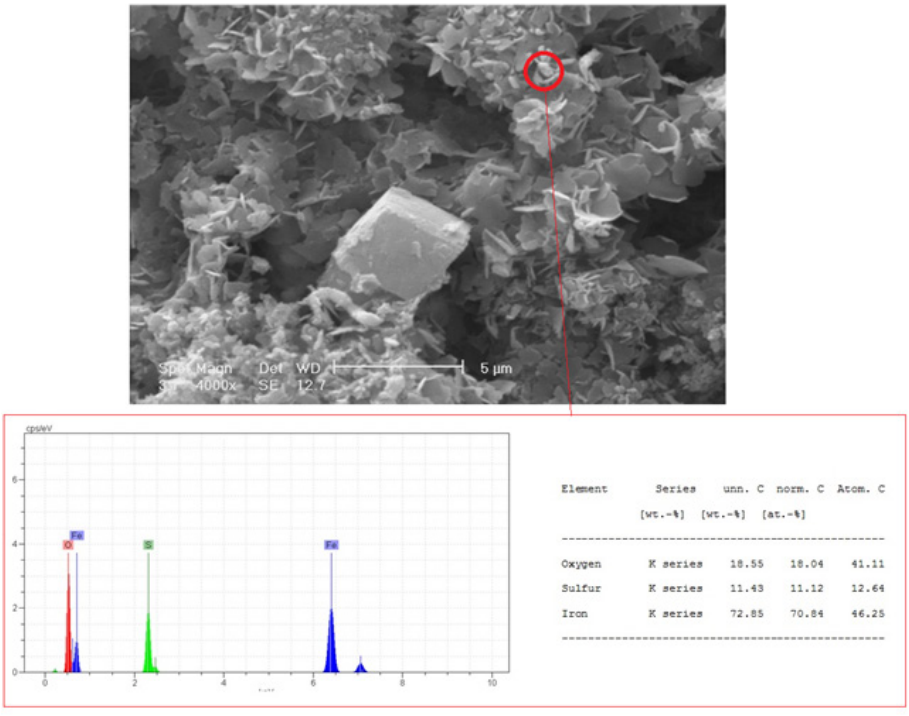

Fig. 6. SEM micrographs of the surface for the sample containing sulfide and carbonate layers at on the 28th day and 0 rpm.

According to the mentioned scenario, the eventual thickening of the mackinawite layer and cracks growth will result in the delamination of the formed layer on the surface. However, as the primary mackinawite transforms into the secondary mackinawite, crack growth, and the surface layer detachment would be prevented., It is possibly, caused by the denser nature and lower RPB ratio of the secondary mackinawite.

It could be observed that with the increase of test duration and re-growth of mackinawite, the sulfide layers transform to each other, and the carbonate layer forms on the surface that finally contributes to the formation of a dense layer on the surface, which could be the reason for decreased corrosion rates. As could be seen in Table 4, the newer sulfide layers have lower R_{PB}, and, as a result, they are denser in comparison to the previous layers.

It should be noted that pH variations during the test indicated a relative pH loss to the range of 4.5-5.5 in the solution with 0 rpm rotational speed in the first two weeks, then pH increased to around 7 while in the fluid with 500 and 1000 rpm rotational speed, it was in the range of 6.5-7.

3.2.3. The thickness of the products layer

As could be seen in Fig. 9 and 10, the SEM micrograph reveals the formation of scale on the surface of the sample after one week for the fluid with 1000 rpm rotational speed. As could be seen, the scale is not continuous and cannot protect the substrate.

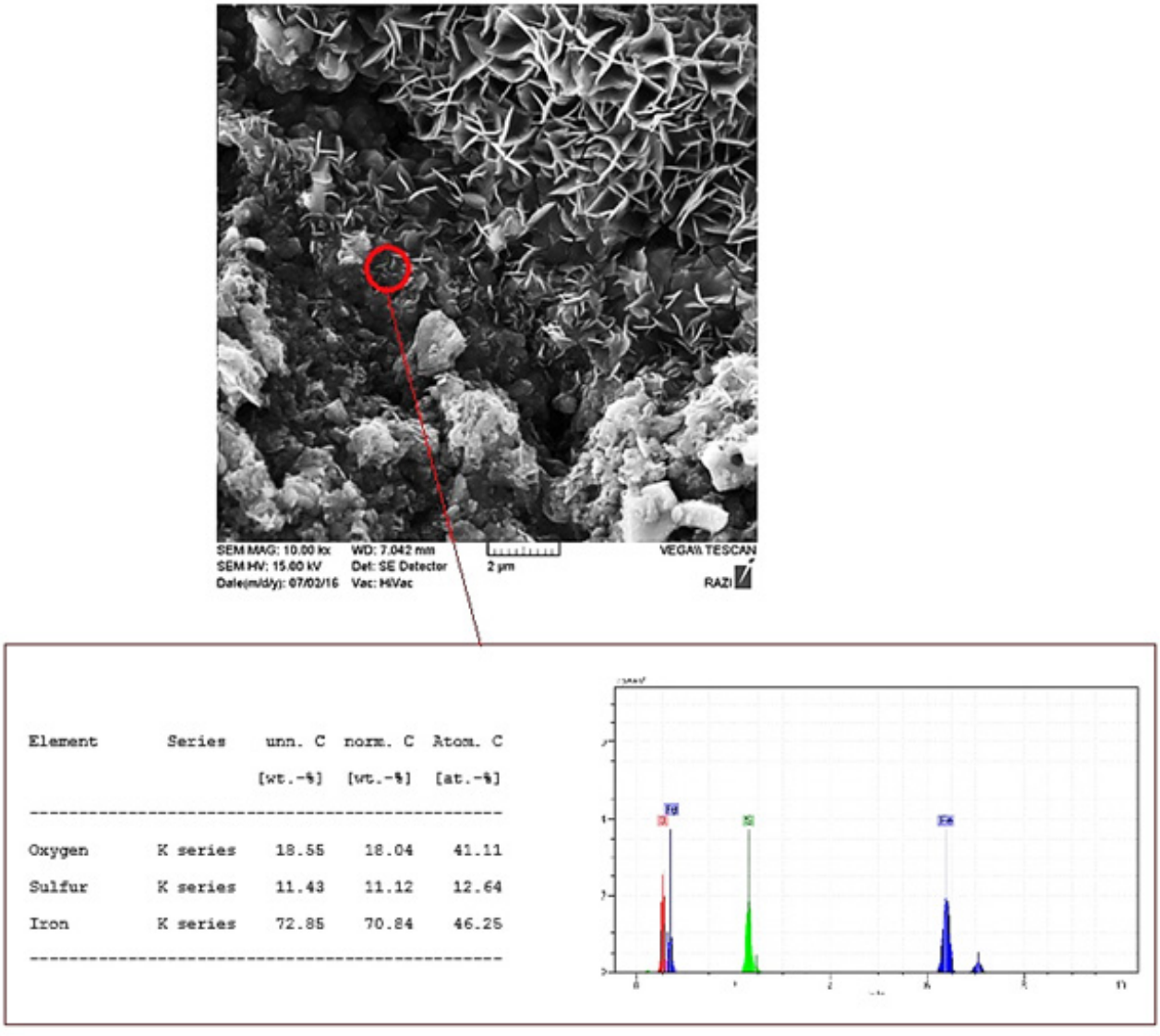

Fig. 7. SEM micrograph of the surface for the sample containing sulfide and carbonate layers on the 28th day and 500 rpm rotational speed.

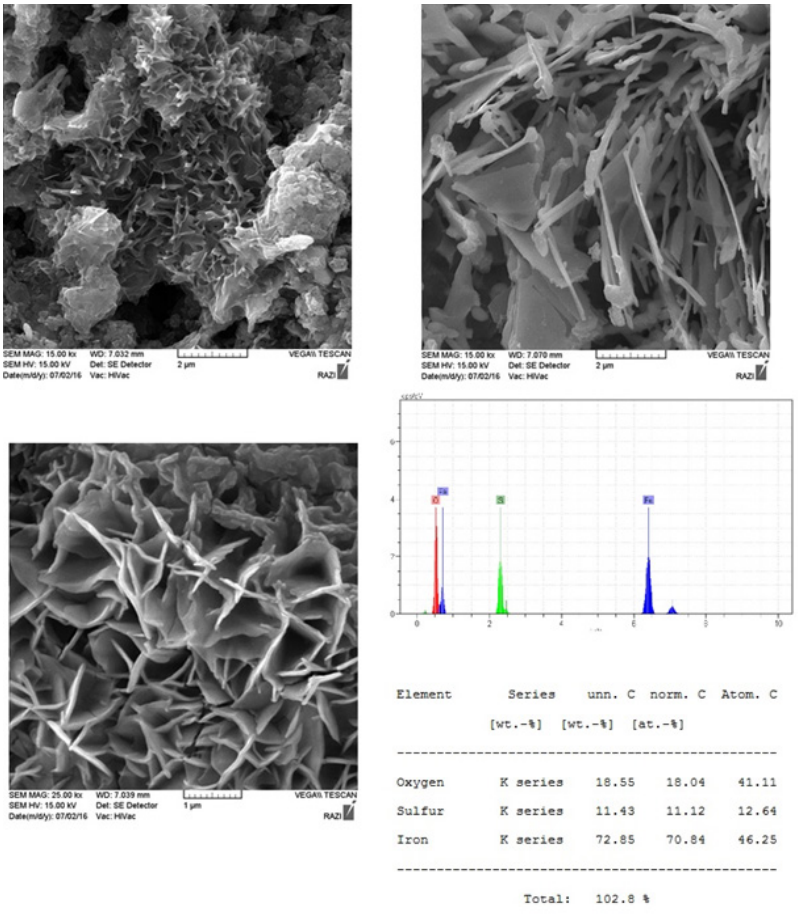

Fig. 8. SEM micrograph of the surface for the sample containing the sulfide layer on the 28th day and 1000 rpm rotational speed.

Table 4. The calculated Pilling-Bedworth ratio for all the layers in different conditions.

	First Mackinawite	Cubic FeS	Second Mackinawite	Greigite	Troilite	Pyrrhotite	Pyrite
Substrate	2.56	0.97	2.197	1.18	1.02	1.05	1.21

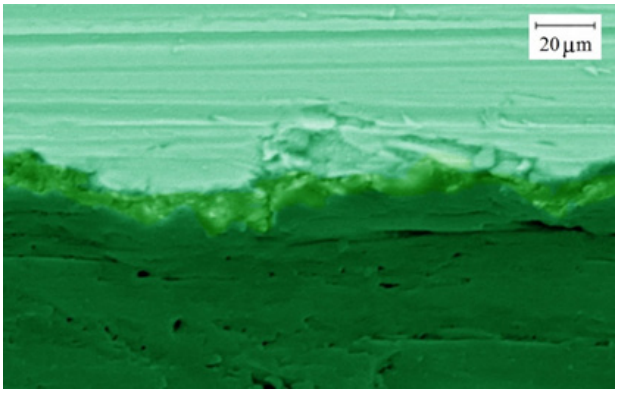

Fig. 9. The variation of the scale thickness on the 7th day and 1000 rpm.

As could be observed in Fig. 10, the scales have been formed in all conditions, and the scale thickness is about 10.2 µm, 14.6 µm, and 15.8 µm for rotational speeds of 0 rpm, 50 rpm, and 1000 rpm, respectively.

As demonstrated in Fig. 10, the scales have been formed in all conditions and have considerably grown and become thicker in all conditions. The thickness of the products in all conditions is presented in table 5.

3.2.4. The formation sites of the new scales

According to the studies carried out by Navabzade et al. [22], the sulfide layer starts with the formation of primary mackinawite, and then they transform to each other. Accordingly, besides the type, the sites of the nucleation and growth of the new layer are amongst the essential factors to determine the adhesion of the scale to the substrate. For example, in the sulfide layer, the nucleation and growth of this layer happen at the substrate/ corrosion products interface due to the higher diffusion rates of sulfide ions in the products layer compared to diffusion rates of iron ions. The remained bubbles or even the burst bubbles on the surface imply the formation of scales at the interface of substrate/ corrosion products. According to the results, these bubbles could be observed on the surface (Fig. 11). These bubbles are related to the produced hydrogen gas evolution as the cathodic reaction product and result in the adhesion of the mackinawite

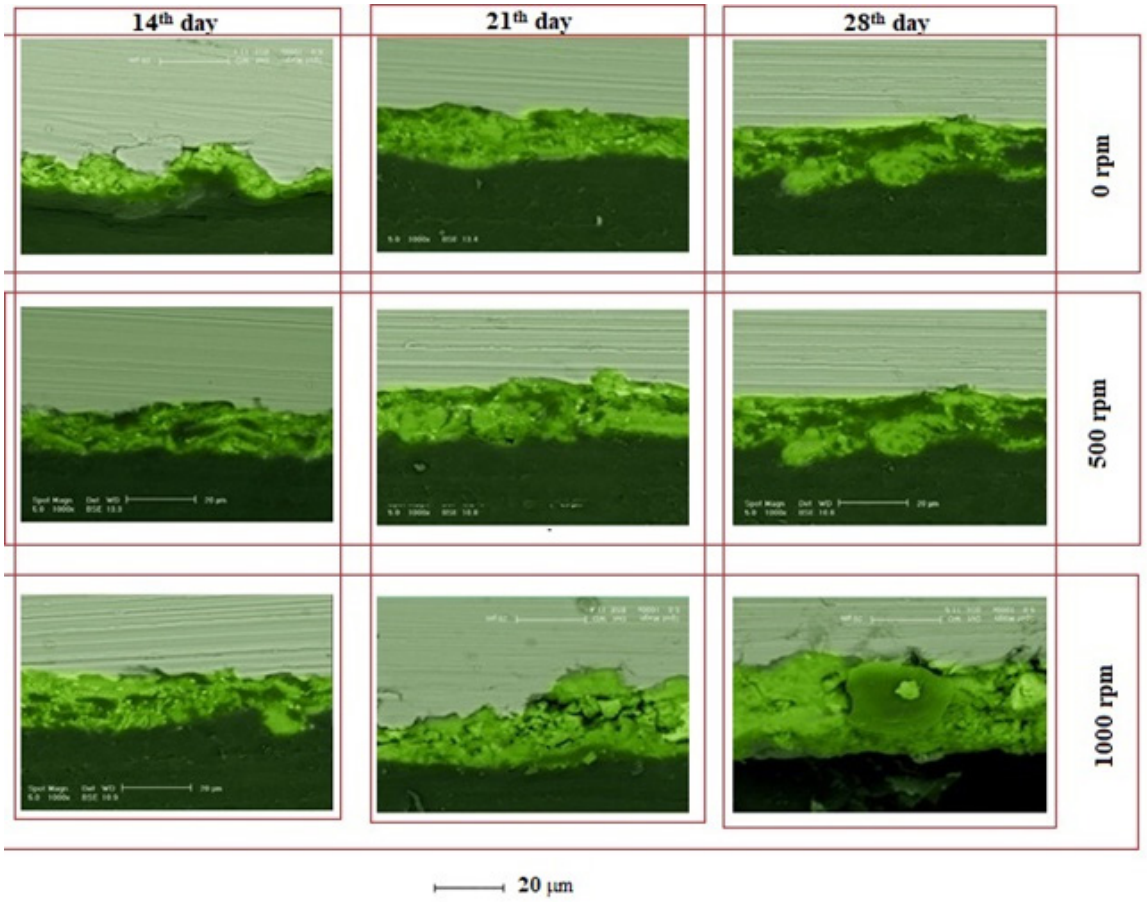

Fig. 10. The SEM micrographs of scale thickness at different times and rotational speed.

Table 5. The thickness of the products in different times and rotational speed (µm)

	Time (Day)		
Rotational Speed (rpm)	14	21	28
0	10.2	14.5	15.4
500	14.6	16.3	16.6
1000	15.8	18.9	27.8

layer to the substrate. The formation sites of new layers could change from substrate/ corrosion products interface to the corrosion products/ fluid interface. The mentioned changes in the formation sites of new layers are due to, first, the transformation of sulfide layers to each other, and second, the changes in compactness of layers, change the diffusion coefficient of them. The variations, as mentioned above, result in the increased adhesion of the surface layer to the substrate surface. For this reason, over time and with the formation of more stable sulfide layers on the surface, these layers have better adhesion to the substrate, besides higher compactness. As could be seen from corrosion results, i.e. section 3.1, the corrosion rate of the substrate decreases over time.

According to the results of SEM micrographs and the values of R_{PB}, it could be concluded that the formation of pyrrhotite and pyrite on the surface contributed to a decreased corrosion rate due to their relatively compact structure. In addition, the XRD results showed that the mentioned layers have been formed at the end of the first, second, and third weeks of immersion at the fluid velocities of 1000, 500, and 0 rpm respectively. All the sulfide layers were detected on the surface after four weeks of immersion. In other words, at the beginning of the corrosion test, the conversion of sulfide layers to each other is dependent on the fluid velocity. In this regard, the required time for the formation of pyrrhotite and pyrite layers and the siderite carbonate scale has decreased with the increase of fluid velocity. However, after the formation of the pyrrhotite and pyrite layers on the surface, the surface conditions for all the fluids have become equal, and the process would become independent of fluid velocity.

It could be observed that with the increase of fluid velocity, the transfer of produced iron ions towards the bulk solution has increased, and as a result, the corrosion rate has increased. In the second step, as the fluid velocity increased, the existing ions in the solution moved faster towards the substrate surface. In other words, the diffusion increased as the fluid velocity increased. In this condition, the surface layers form with higher rates, and as a result, the slope of the curve (corrosion rate versus time) increases in this step. Finally, an increase in the fluid velocity in the third step leads to the increased corrosion product growth, and this contributes to the compactness in shorter times in which it causes the stabilization of corrosion rate at a specified value (plateaued curve).

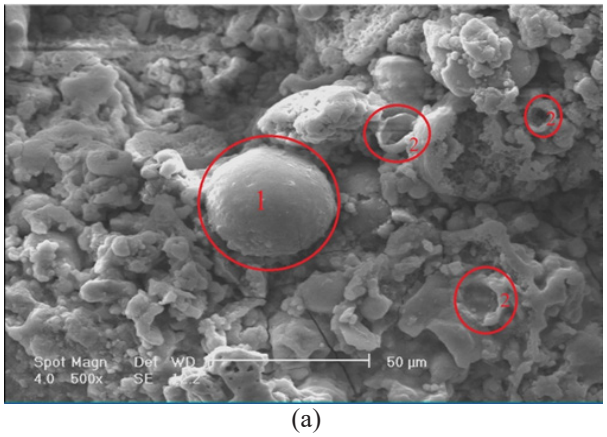

(a)

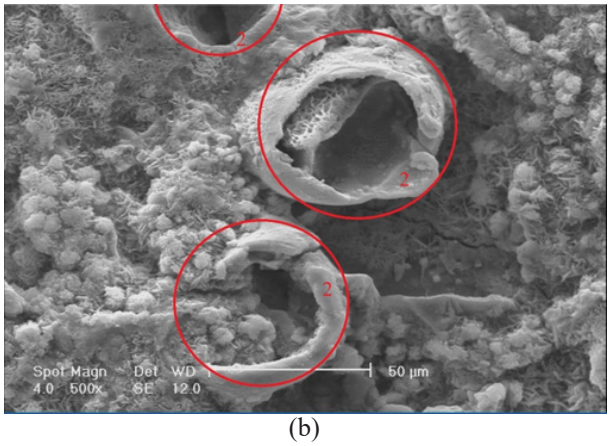

(b)

Fig. 11. a) The formation and trapping of the hydrogen bubble underneath the surface layer b) Scale damage through a hydrogen bubble collapse underneath the surface.

3.3. The effect of fluid velocity on the corrosion rate

According to Fig. 12, there are 4 steps for corrosion progress that in the first step, the diffusion through the porous and non-adhesive layers controls the corrosion rate and the corrosion rate has increased in this step. After this step, the formation of more compact layers on the surface resulted in the decreased diffusion through this layer, and it is predicted that the reaction mechanism has changed from diffusion through porous products to diffusion through compact products (the second step). In this condition, due to the nature of the new layers, the corrosion rate has decreased over time. In longer times and with the formation of all the sulfide layers and the formation of carbonate layers on the surface, the corrosion rate has become constant at a specified rate (the third step). The diffusion rate in corrosion products controls the corrosion rate. Of course, as time passes, the nature of the corrosion products has the maximum effect on the corrosion rate by affecting the ions diffusion rate.

As Fig. 13 Shows, it is reasonable to deduce that the fluid velocity affects the corrosion rate, by affecting the formation rate and transformation of corrosion products to each other (including sulfide and carbonate layers) and also the corrosion rate variations. In this condition, with the increased fluid velocity, the decrease or increase in the corrosion rate (the first and second steps) would happen with higher rates. Nevertheless, as time passes and more compact and adherent products form on the surface, the corrosion rate becomes constant, and the fluid velocity would not have any effects on the corrosion rate.

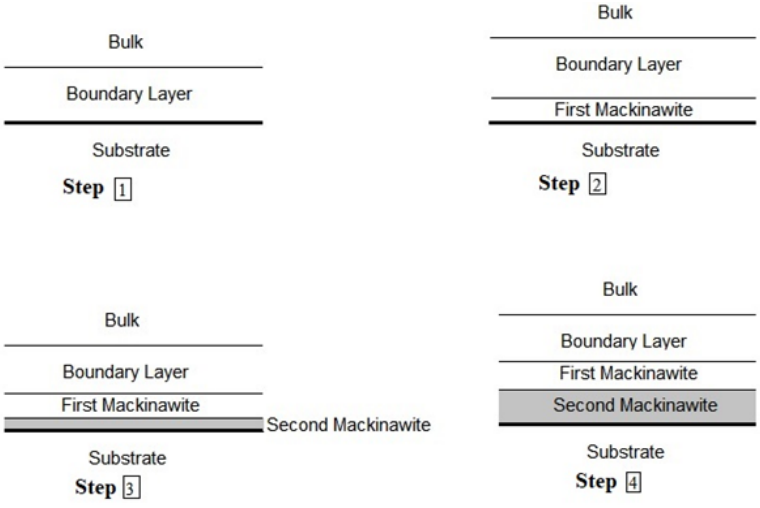

Fig. 12. A schematics of the corrosion steps and the formation of scales on the steel surface.

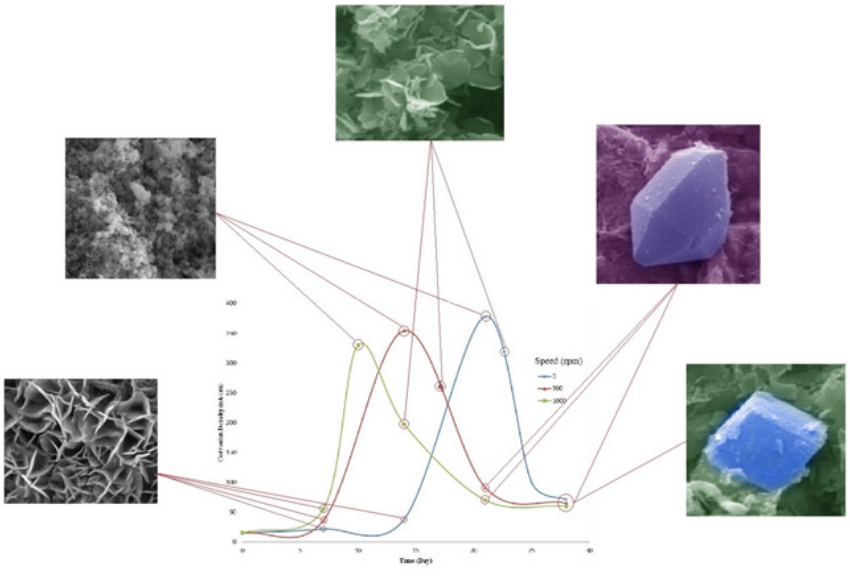

Fig. 13. The formation of various sulfide layers on the substrate at different times and its effect on the corrosion rate.

3.4. Mechanism of corrosion

3.4.1. The variations of iron ions concentration

In current research, the variations of iron ions concentrations were used as a criterion for investigating the kinetics of the steel substrate surface reactions. The variations of iron ion concentration were measured in 28 days in an aqueous solution for different fluid velocities. Also, temperatures and the related graphs were plotted (Fig. 14 and Table 6). According to the variations of iron ion concentration during this period, the reaction fraction variations (α) with time are similar to the variations of iron ion concentration.

In the following, this reaction was evaluated using the g (α) equations related to various kinetics models. For this purpose, by placing the (α) and t in the mentioned reactions, the g (α) – t graphs were plotted.

Table 6. The variations of iron ion concentration in different conditions.

	298 K			318 K		338 K	
Time (Day)	0 (rpm)	500 (rpm)	1000 (rpm)	0 (rpm)	1000 (rpm)	0 (rpm)	1000 (rpm)
0	0	0	0	0	0	0	0
1	0.363832	0.4041	0.4423	0.3733	0.509	0.3785	0.5875
3	0.654898	0.6875	0.7031	0.621911	0.714243	0.4831	0.731143
6	0.7527	0.81	0.9128	0.734985	0.9201	0.5854	0.9254
8	0.7815	0.8387	0.9389	0.830392	0.9541	0.6435	0.9515
10	0.8288	0.893931	0.9591	0.85	0.9615	0.6854	0.9625
14	0.8508	0.9329	0.9683	0.87	0.9685	0.7851	0.9674
16	0.8893	0.9538	0.97	0.89	0.9723	0.8648	0.9723
18	0.90827	0.9725	0.975	0.9187	0.9754	0.9365	0.9768
21	0.9237	0.9818	0.98	0.93	0.9796	0.9513	0.9837
23	0.9563	0.9864	0.983	0.95	0.9816	0.9625	0.9875
25	0.9774	0.9915	0.986	0.97	0.9879	0.97	0.9915
27	0.9829	0.9972	0.995	0.99	0.99	0.98	0.9981
28	1	1	1	1	1	1	1

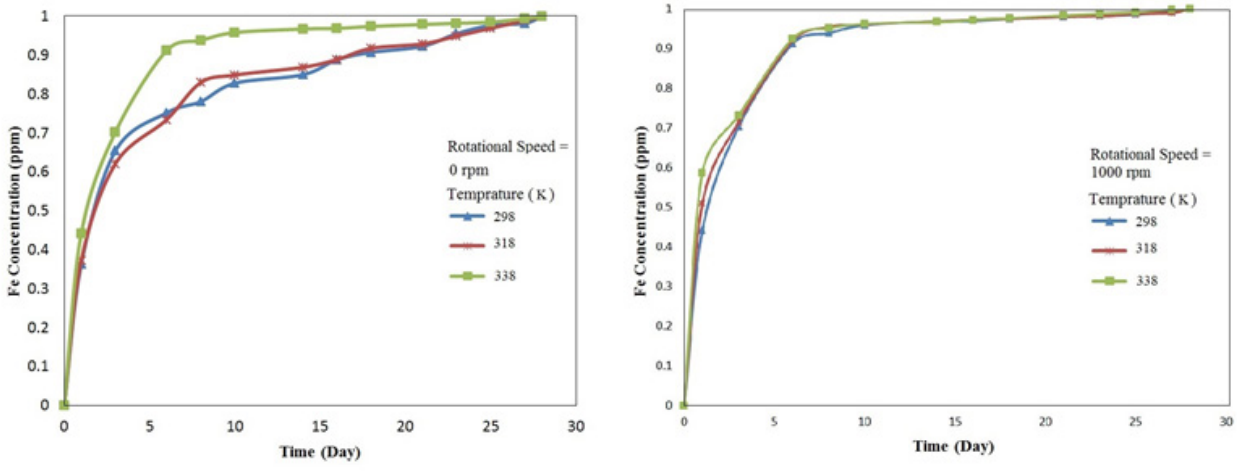

Fig. 14. The variations of iron ion concentration and the reaction fraction with time at different fluid velocities and temperatures.

3.4.2. Kinetics analysis

The results of the isothermal iron change in the aqueous system can be used to calculate the kinetics parameters of the investigated process. The fractional reaction (a) can be easily specified by iron change curves using the following equation [23-25]:

$$\alpha = \frac{m_t - m_i}{m_f - m_i} \quad \text{Eq. (1)}$$

Where, m_i, m_f, and m_t are the initial, final, and current sample mass at the moment t, respectively. The curve of (α) versus T can be used for the kinetics analysis and the description of the reaction mechanism. For this reason, it is possible to analyze the isothermal kinetics data by combining the following equations:

(I): The differential form of the kinetics equation:

$$\frac{d\alpha}{dt} = k\, f(\alpha) \quad \text{Eq. (2)}$$

Where t is the time, k is the reaction rate constant, and f (α) is an algebraic function dependent on the reaction mechanism (or differential reaction model).

(II): The Arrhenius equation:

$$k = A.\exp(\frac{-Q}{RT}) \quad \text{Eq. (3)}$$

Where T and R parameters are absolute temperature and gas constant, respectively.

$$\frac{d\alpha}{dt} = A.\exp(\frac{-Q}{RT})\, f(\alpha) \quad \text{Eq. (4)}$$

So:

$$\frac{d\alpha}{f(\alpha)} = A.\exp(\frac{-Q}{RT})\, dt \quad \text{Eq. (5)}$$

After integrating this equation, the following equation could be obtained:

$$\int_0^{\alpha} \frac{d\alpha}{f(\alpha)} = \int_0^{t} k dt \quad \text{Eq. (6)}$$

Moreover:

$$\int_0^{\alpha} \frac{d\alpha}{f(\alpha)} = g(\alpha) \quad \text{Eq. (7)}$$

Finally:

$$g(\alpha) = k.t \quad \text{Eq. (8)}$$

Some of the common solid-state reactions are presented in Table A. The equation(2) can be used for different temperatures to determine the Q parameter, therefore:

$$k_1 = A \times \exp(\frac{-Q}{RT_1}) \quad \text{Eq. (9)}$$

Then:

$$\ln k_1 = \ln A - (\frac{Q}{R})\frac{1}{T_1} \quad \text{Eq. (10)}$$

And by plotting the ln(k) versus $\frac{1}{T}$ curve, $(-\frac{Q}{R})$ would be the curve slope and kinetics triplet, A, Q, and f(α) or g(α) would be obtained.

This section will study the g(α)-t graphs which were plotted for kinetics models, and their deviations from the linear state have been used as the performance criteria for each of these models. According to the plotted graphs, it was observed that the minimum deviation from the linear state was attributed to equations related to the diffusion control mechanism. As could be seen in Table 7, the equations of two-dimensional diffusion have the least deviation from the linear state among the diffusion equations. As a result, the two-dimensional diffusion (via the boundary layer of the corrosion products) with the g(α)=(1-α)ln(1-α)+α equation is the governing equation of corrosion rate.

It is necessary to determine the slope of the g(α)-t curves precisely to determine the activation energy at two different velocities. By determining the slope of the ln k-(1/T) curve (Fig. 15), the activation energy of the reaction for the fluid velocities of 0 and 1000 rpm could be obtained. The calculated activation energies for the two velocities are 646.47 J/mol and 2743.41 J/mol, respectively.

According to the calculations, the activation energy has increased from 646.47 J/mol to 2743.41 J/mol as the fluid velocity increased. It could be said this increase is due to a change in the diffusion mechanism which controls the reaction rate. As mentioned in the thermodynamic evaluation section, the increase in the fluid velocity has increased the formation and transformation rate of sulfide layers. As a result, with the formation of a dense and compact sulfide layer, the diffusion rate in this layer has decreased and the activation energy for the formation of the new layer has increased.

Finally, it could be said that in the beginning, the increased fluid velocity accelerates the corrosion rate variation by faster porous layers formation.

Table 7. The R^2 related to the plotted graphs for various g(α) equations.

Temperature →		298 K		318 K		338 K	
Model ↓		0 rpm	1000 rpm	0 rpm	1000 rpm	0 rpm	1000 rpm
diffusional control	one dimensional	0.9276	0.9256	0.9528	0.9438	0.9588	0.9598
	two dimensional	0.9934	0.995	0.9917	0.9909	0.9975	0.9975
	Ginstling	0.9974	0.9434	0.979	0.9553	0.9729	0.968
Sigmoidal	A2	0.7947	0.7899	0.7868	0.7893	0.7918	0.8085
	A3	0.737	0.7362	0.7048	0.723	0.723	0.723
	A4	0.8232	0.8137	0.8483	0.8283	0.8486	0.867
	B1	0.6926	0.68	0.7392	0.7067	0.7487	0.775
Order with respect to alpha	Zero-order	0.807	0.8011	0.822	0.8044	0.8146	0.8202
	First Order	0.8303	0.8177	0.8673	0.8407	0.8724	0.8923
	Second Order	0.8582	0.8382	0.9063	0.8769	0.9212	0.9507
Geometric model	Interface (Contracting Area)	0.8186	0.8096	0.8457	0.8235	0.8235	0.8235
	Interface (Contracting Volume)	0.8224	0.8122	0.8531	0.8293	0.8544	0.8694
	Interface	0.8148	0.8069	0.838	0.8174	0.8352	0.8454
Power Law	Half Power	0.7403	0.7399	0.7151	0.7157	0.7033	0.7055
	Third Power	0.6697	0.6711	0.6367	0.6415	0.6258	0.6269
	Quarter Power	0.6181	0.6199	0.5864	0.5919	0.5769	0.5777

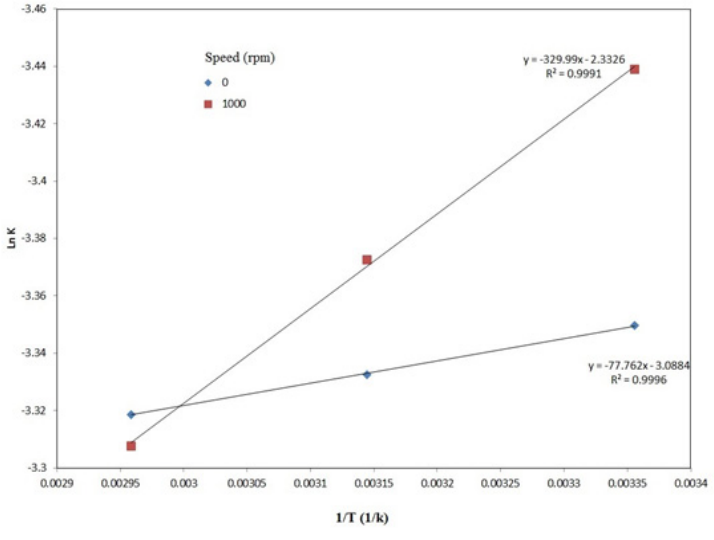

Fig. 15. The variations of ln k versus 1/T (1/k).

However, with the formation of a dense layer, the effect of fluid velocity increase would become negligible. In this condition, the corrosion rate is equal for all the three fluids.

4. Conclusion

Based on the studies conducted in this study, it was observed that:

- The mackinawite layer could not protect the substrate due to poor adhesion and acicular structure.
- After the formation of the primary mackinawite layer of the substrate, the other sulfide species and siderite would form at the interface of primary mackinawite and steel substrate and decrease the corrosion rate due to the formation of a dense layer on the surface.
- The controlling mechanism was the second-order diffusion, which has resulted in the increased activation energy as the fluid velocity has increased. This prediction was due to the change in the diffusion path from porous corrosion products layer to dense corrosion product layer and the formation of a protective layer at higher fluid velocities, i.e., 1000 rpm.
- At first, the corrosion rate-controlling parameter waz the diffusion rate through the porous corrosion products layer. After the formation of the dense corrosion products layer, the diffusion through this layer would be the rate-controlling parameter.
- In the stagnant solution, the diffusion mechanism was through porous corrosion products with the activation energy equal to 646.47 J/mol and the equation of $g(\alpha) = (1-\alpha) \ln (1-\alpha) + \alpha$.
- In the fluid with 1000 rpm rotational speed, the diffusion mechanism was through porous corrosion products with the activation energy equaled 2743.41 J/mol and the equation of $g(\alpha) = (1-\alpha) \ln (1-\alpha) + \alpha$.
- At first, the increased fluid velocity resulted in an increased corrosion rate due to the acceleration of the formation of porous corrosion products.
- Over time and due to the formation of dense/ compact corrosion product layer, the corrosion rate became constant (plateau curve), and the effect of the fluid velocity became negligible.

References

[1] J. Sun, C. Sun, G. Zhang, X. Li, W. Zhao, T. Jiang, H. Liu, X. Cheng, Y. Wang A, Corros. Sci. , 107 (2016): 31-40.

[2] A. Dugstad, B. Morland, S. Clausen, Corrosion Conference, (2011), Paper No. 11070, NACE, Houston, TX.

[3] I.S. Cole, P. Corrigan, S. Sim, N. Birbilis, INT J GREENH GAS CON, 5.4 (2011): 749-756.

[4] A. Kahyarian, M.Achour, S. Nesic, Corrosion Conference, Houston Tx, (2017): 149-190.

[5] J. Kvarekval, R. Nyborg, H. Choi, Corrosion Conference, Paper No. 03339, NACE, Houston, TX, (2003).

[6] I.H. Omar, Y.M. Gunaltun, J. Kvarekval, A. Dugstad, Corrosion Conference, Paper No.05300, NACE, Houston, TX, (2005).

[7] A.S. Ruhl, A. Kranzmann, Int. J. Greenh. Gas Control 9 (2012) 85-90.

[8] Y.S. Choi, S. Nesic, Corrosion Conference, Paper No.10196, NACE, Houston, TX, (2010).

[9] Nešić, S., Postlethwaite, J., & Olsen, S., Corros, 52.4 (1996) 280-294.

[10] D.W.Shoesmith, P. Taylor, M.G. Bailey, D. Owen, J. Electrochem. Soc., 127.5 (1980): 1007.

[11] S. Navabzade Esmaeely, G.Bota, B. Brown, S.Nesic, Corrosion Conference, Houston Tx, 74.1 (2018): 37-49.

[12] W. Sun and S. Nesic, Corrosion Conference, Paper No. 07655, 19 (2007).

[13] Champion Technologies: "Corrosion Mitigation for Complex Environments". Houston: Champion Technologies; (2012).

[14] AJ. Brito, AT.Dealmeida,, Reliab. Eng. Syst. 94.2 (2009) 187-198.

[15] S. Nesic, H. Li, J. Huang, D. Sormaz, Corrosion Conference, Paper No. 09572, (2009).

[16] W. Sun, S. Nesic, Corrosion, 65.5 (2009) 291-307.

[17] Y.S. Choi, S. Nesic, S. Ling, Electrochim. Acta, 56.4 (2011) 1752-1760.

[18] P.C. Okonkwo, M.H. Sliem, R.A. Shakoor, J. Mater. Eng 26.8 (2017) 3775-3783.

[19] N. Yaakob, F. Farelas, M. Singer, S. Nesic, D. Young, Corrosion Conference, Paper No. 7695, (2016).

[20] B. Brown, "H2S/CO2 Corrosion in Multiphase Flow", Ohio University Advisory Board Meeting Report, Internal Report to be Published, 2006.

[21] M. Schutze, "Protective Oxide Scales and Their Breakdown", John Wiley & Sons, Chichester, (1997).

[22] S. Navabzade Esmaeely, W. Zhang, B. Brown, Corrosion Conference, Houston Tx, 73.9 (2017) 1098-1106.

[23] M. Schoenitz, B. Patel, O. Agboh and E. L. Dreizin, Thermochimica Acta 507 (2010): 115-122.

[24] R. F. Speyer, "Thermal Analysis of Materials", Marcel Dekker Inc., New York, (1993).

[25] M. Schoenitz, C. M. Chen, X. Zhu, and E. L. Dreizin, 40th International Conference of ICT, Karlsruhe, Germany, 34 (2009) 1–11.

[26] N. Pilling and R. Bedworth, J. Inst. Metals, 29 (1923) 529.

[27] R. Winston Revie, H. Uhlig, "Corrosion and Corrosion Control", 4th Edition.

[28] M. Golahan, D. Young, M. Singer, and R.P. Nogueira, "Black Powder Formation by Dewing and Hygroscopic Corrosion Processes", J Nat Gas Sci Eng, 56 (2018): 358-367.

Appendix A

One of the most common parameters for studying the porosity and adhesion of the corrosion products to the substrate is the R_{PB}. This ratio is used as a factor to evaluate the specifications of corrosion products.
The R_{PB} [26] is the ratio of the volume of the elementary cell of product to the volume of the elementary cell of the metal. R_{PB} is defined as:

$$R_{PB} = \frac{V_{Product}}{V_{metal}} = \frac{M_{Product} \cdot \rho_{metal}}{nM_{metal} \cdot \rho_{Product}} \quad \text{Eq. (11)}$$

Where

• R_{PB} is the Pilling–Bedworth ratio,
• M: the atomic or molecular mass,
• n: number of atoms of metal per one molecule of the product
• ρ: density, and
• V: Volume.

Based on measurements, the following relationships can be shown:
• $R_{PB} < 1$: The product layer is too thin, likely broken, and provides no protective effect.
• $R_{PB} > 2$: The product layer chips off and provides no protective effect.
• $1 < R_{PB} < 2$: The product layer is passivating and provides a protecting effect against further surface oxidation.
However, the exceptions to the above R_{PB} rules are numerous. Many of the exceptions can be attributed to the mechanism of the product growth: the underlying assumption in the R_{PB} is that oxygen has to diffuse through the product layer to the metal surface; indeed, it is often the metal ion that diffuses to the air-product interface [27].
However, according to some research [12, 28], this method can be used for sulfide scales. For example, according to Sun and Nesic [12], micro-cracks on the Mackinawite surface is due to the differences between Mackinawite volume and iron volume (R_{PB} =2.56) which is the reason for internal compressive stresses.

APPENDIX B

Table A: Some of the equations suggested for solid-state reactions

No.	Model	Symbol	Differential form, $f(\alpha)$	Integral form, $g(\alpha)$
1	Power law	P1	$4\alpha^{3/4}$	$\alpha^{1/4}$
2	Power law	P2	$3\alpha^{2/3}$	$\alpha^{1/3}$
3	Power law	P3	$2\alpha^{1/2}$	$\alpha^{1/2}$
4	Power law	P4	$2/3\alpha^{-1/2}$	$\alpha^{3/2}$
5	Exponential law	E1	α	$\ln\alpha$
6	Avrami–Erofeev ($m = 2$)	A2	$2(1-\alpha)\,[-\ln(1-\alpha)]^{1/2}$	$[-\ln(1-\alpha)]^{1/2}$
7	Avrami–Erofeev ($m = 3$)	A3	$3(1-\alpha)\,[-\ln(1-\alpha)]^{2/3}$	$[-\ln(1-\alpha)]^{1/3}$
8	Avrami–Erofeev ($m = 4$)	A4	$4(1-\alpha)\,[-\ln(1-\alpha)]^{3/4}$	$[-\ln(1-\alpha)]^{1/4}$
9	Prout–Tompkins	B1	$\alpha(1-\alpha)$	$\ln[\alpha/(1-\alpha)]$
10	Contracting area	R2	$2(1-\alpha)^{1/2}$	$1-(1-\alpha)^{1/2}$
11	Contracting volume	R3	$3(1-\alpha)^{2/3}$	$1-(1-\alpha)^{1/3}$
12	One-dimensional diffusion	D1	$1/2\alpha$	α^2
13	Two-dimensional diffusion	D2	$[-\ln(1-\alpha)]^{-1}$	$(1-\alpha)\ln(1-\alpha)+\alpha$
14	Three-dimensional diffusion	D3	$3/2(1-\alpha)^{2/3}[1-(1-\alpha)^{1/3}]$	$[1-(1-\alpha)^{1/3}]^2$
15	Ginstling–Brounstein	D4	$3/2[(1-\alpha)^{-1/3}-1]^{-1}$	$1-(2\alpha/3)-(1-\alpha)^{2/3}$
16	Zero order reaction	F0	1	α
17	First order reaction (Mampel)	F1	$1-\alpha$	$-\ln(1-\alpha)$
18	Second order reaction	F2	$(1-\alpha)^2$	$[1/(1-\alpha)]-1$
19	Third-order reaction	F3	$(1-\alpha)^3$	$[1/(1-\alpha)^2]-1$